ELSEVIER

Polymer 41 (2000) 277–284

polymer

Depth-profiles of structure in single- and multilayered commercial polymer films using grazing-incidence X-ray diffraction

N.S. Murthy*, C. Bednarczyk, H. Minor

AlliedSignal Inc., Research and Technology, P.O. Box 1021, Morristown, NJ 07962, USA

Received 24 July 1998; received in revised form 9 February 1999; accepted 10 February 1999

Abstract

Grazing-incidence X-ray diffraction is used to analyze the variation in structural features—such as crystalline index and crystallite size-perfection (CI and CSP)—with depth in several commercially relevant mono- and multi-layer polymer films. The CI and CSP at the casting-roll surface of a melt-cast and biaxially oriented nylon 6 (N6) film is the same as in the bulk, but the air-exposed surface has lower CI and CSP than the bulk. These differences are attributed to the influence of the initial crystallization behavior at the two surfaces (roll-surface poorly ordered than the air-surface) on the eventual crystallinities observed after drawing. In a bilayer laminate of poly(chlorotrifluoro ethylene) (PCTFE), and poly(ethylene–ethyl acrylate) (EEA), the CI is lower but the CSP of PCTFE appears to be higher at the interface between PCTFE and EEA. The technique was able to find differences in the PE unit cell volume within the PE layer at the air/PE and PE/N6 interface in a three-layer film (PE/N6/PE). The method was also used to monitor the variation in preferred orientation with depth in the aluminum layer deposited on polymer films in a multilayered structure, as well as to examine the thin surface coatings. © 1999 Elsevier Science Ltd. All rights reserved.

Keywords: Grazing-incidence diffraction; Single- and multilayered films; Crystallinity

1. Introduction

Multilayered polymer films are commonly produced by either coextrusion or lamination. Such films are now being increasingly used to take advantage of the unique characteristics of different polymers. For example, coextrusion of a poly(ethylene/ethylene acrylate) (EEA, a low melting point polymer) with poly(chlorotrifluoro ethylene) (PCTFE, an excellent barrier) yields a sealable high-barrier film. A laminate of nylon 6 (N6) and polyethylene (PE) provides both superior oxygen barrier (because of N6) and good moisture barrier (because of PE). Grazing-incidence diffraction (GID) is a unique tool for studying the structure at the surfaces, interfaces and within each of the layers as a function of depth without delamination. These measurements are useful for evaluating the adhesion between layers in multilayer structures and for studying the performance of these films.

X-ray diffraction (XRD) measurements from unoriented polymers are routinely carried out in reflection mode. In this geometry, the X-rays penetrate into the sample a distance ~1 mm, and thus the data obtained has information about the bulk structure of the material. If the surface of the sample is set at a small angle (~1°) relative to the direction of the incident beam, the *distance traversed by the beam* within the sample increases by orders of magnitude. As a result, the effective *depth of penetration* of X-rays perpendicular to the surface decreases as the angle of incidence decreases up to the critical angle limit (~0.017° for CuKα for polymers like nylon 6) at which total reflection occurs. Thus, GID provides information about the structure near the surface [1–2]. GID has been used extensively to study compositional variations in semiconductors [3–5], residual stresses metals [6,7] and surface and interfacial structure in polymers [8–12]. A related technique, X-ray and neutron reflectivity, is also widely used to study polymer surfaces and interfaces [13–15]. Here we use GID to selectively analyze the scattering from layers close to the surface, and illustrate the use of such surface-enhanced X-ray diffraction measurements for studying the variation with depth of the composition and structure in commercially produced multilayer films.

2. Materials and methods

The following samples were studied: (1) A biaxially

---

* Corresponding author.
E-mail address: nsmurthy@alliedsignal.com (N.S. Murthy)

PII: S0032-3861(99)00137-8

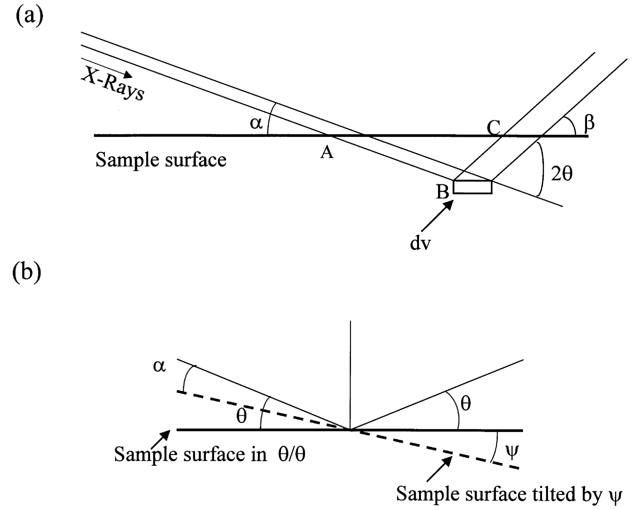

Fig. 1. Diffraction geometry used in data collection and the definition of various terms.

oriented N6 film. (2) A two-layer laminate made from PCTFE, and EEA. (3) A three-layer laminate made by sandwiching a layer of biaxially oriented N6 between two layers of PE. (4) A four-layer laminate made by sandwiching a layer of aluminum (Al) between two layers of N6, and an outside layer of EEA. Samples 1, 3 and 4 were made with AlliedSignal's biaxially oriented N6 and sample No. 2 is from Sumitomo, Japan.

X-ray diffraction data (XRD) were collected by using a Huber two-circle diffractometer on beam lines X18B and X16B at the National Synchrotron Light Source, Brookhaven National Laboratory. The wavelength (λ) was selected using a channel cut (220) silicon monochromator and the beam-size was defined by using two pairs of slits, one near the hutch–entrance and the other near the sample. The wavelength was ~0.16 nm (see caption to Fig. 2 for actual values). The films were held flat on a glass slide using adhesive tapes away from the area of irradiation. Care was taken to ensure that there were no wrinkles in the films. The sample was tilted to various angles of incidence (α) and the scattered intensities were recorded as a function

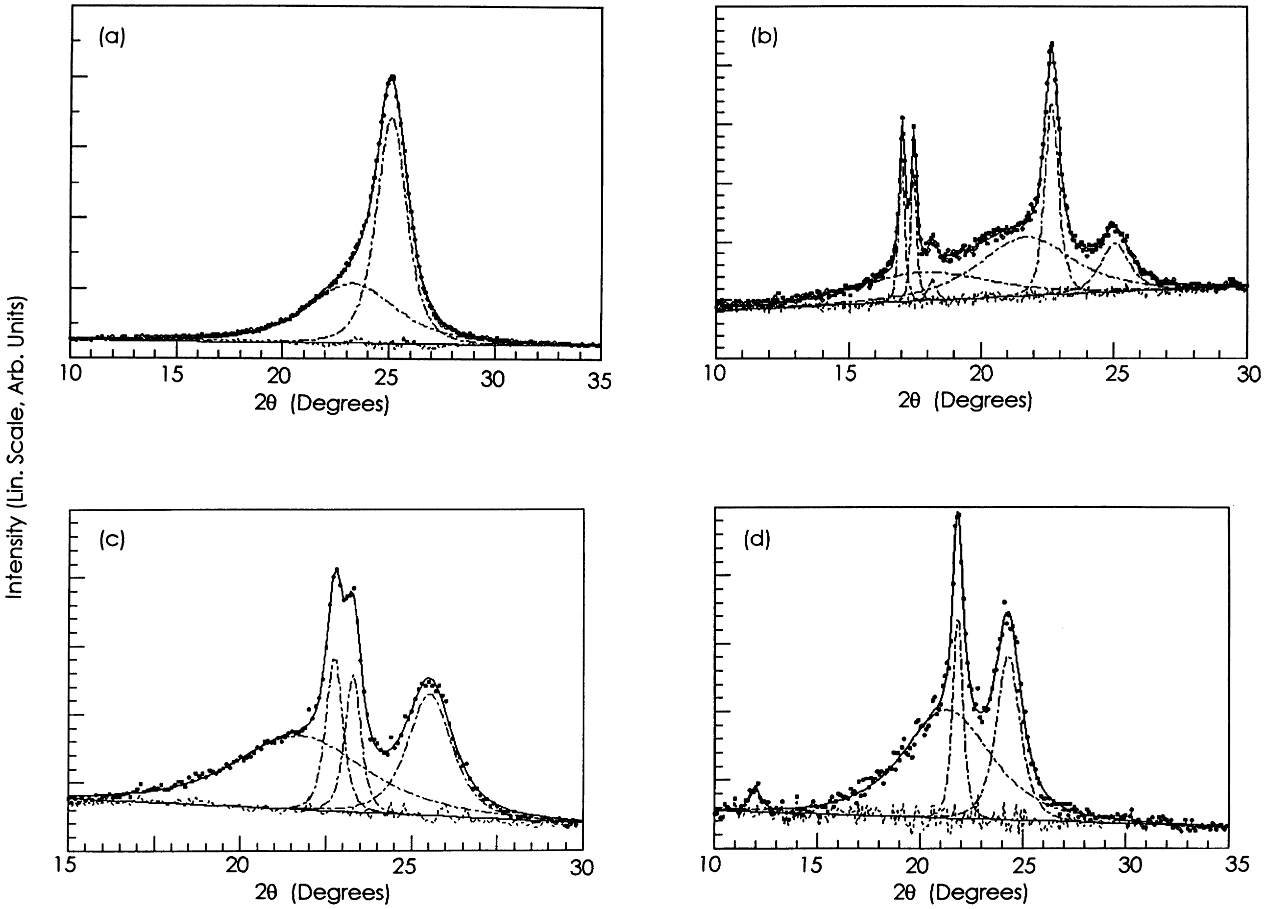

Fig. 2. Examples of profile fitted plots: (a) A single layer of biaxially oriented nylon 6 at $\alpha = 1°$, $\lambda = 1.628$ Å; (b) A bilayer of EEA and PCTFE at $\alpha = 8°$, $\lambda = 1.628$ Å; (c) Three layer laminate of PE/N6/PE at $\alpha = 0.5°$, $\lambda = 1.653$ Å; (d) A four layer structure made of N6/Al/N6/EEA from the PE side at $\alpha = 1°$, $\lambda = 1.576$ Å. In this and in Figs. 4, 6 and 7, the small circles are the observed data, the full line through these circles is the fitted data. The fitted data is the sum of the components shown by broken lines. The broken line near the base-line (solid-line) is the residue or the difference between the observed data and the fitted curve.

of the scattering angles (2θ) as shown in Fig. 1. Two sets of data were collected on all the samples; the first set of data were collected using a Soller slit, and the second set were collected using a germanium monochromator in the diffracted beam. We here present data obtained with a monochromator for the biaxially oriented N6 film and the EEA/PCTFE bilayer, and the data obtained with a Soller slit for the PE/N6/PE and N6/Al/N6/EEA laminates.

The scans were curve-fitted using a modified version of the program SHADOW [16,17]. Examples of the profile analyses of the four samples are shown in Fig. 2. The results of these profile analyses were used to calculate a measure of crystallinity in the form of a crystalline index (CI), and of the size and defects within the crystals in the form a crystallite size and perfection (CSP) parameter. CI is the ratio of the area under the crystalline peaks and the total area over the angular range of the data. This angular range was selected so as to cover all the intense crystalline peaks. CSP is the Scherrer size calculated from the expression [18]:

$$\mathrm{CSP} = \frac{0.9\lambda}{\Delta\theta\cos(2\theta)}. \tag{1}$$

Depth of penetration τ was calculated from the relation [19]:

$$\tau = \frac{\sin^2\theta - \sin^2\psi}{2\mu\sin\theta\cos\psi}, \tag{2}$$

$$\alpha = \theta + \psi, \tag{3}$$

where α is the angle of incidence, θ is one-half the scattering angle, and ψ is the tilt-angle (Fig. 1). ψ is positive when measured in the same direction as θ. Thus, large negative ψ as indicated in the figure (but less than the absolute value of θ) gives a small angle of incidence (α) and small τ. μ is the linear absorption coefficient. τ is a convenient measure of irradiated depth (where the intensity is reduced to $1/e$) and is not the depth z beneath the surface. τ is calculated by expressing the beam path L as

$$L = AB + BC = z\left(\frac{1}{\sin\alpha} + \frac{1}{\sin\beta}\right), \tag{4}$$

and by defining τ by the condition $z = \tau$ when $\mu L = 1$ [7]. When the beam passes through two layers with path lengths of a and b, then an average μ can be written as

$$\mu = \frac{a\mu_a + b\mu_b}{a + b}, \tag{5}$$

where μ_a and μ_b are the linear absorption coefficients, and a and b are the X-ray path length in the two layers a and b, respectively. Alternatively, the penetration depth can be calculated from the surface of each layer, the upper layer being regarded as just an absorber in the path of the beam.

Eq. (2) is valid at $\alpha \gg \alpha_c$, where α_c is the critical angle. At $\alpha \sim \alpha_c$, the penetration depth is given by [1,9,19]:

$$\tau = \sqrt{2}\left(\frac{\lambda}{4\pi}\right)\left\{\left[\left(\alpha^2 - \alpha_c^2\right)^2 + (2\beta)^2\right]^{1/2} - \left(\alpha^2 - \alpha_c^2\right)\right\}^{-1/2}, \tag{6}$$

$$\beta = \frac{\lambda\mu}{4\pi}, \tag{7}$$

$$\alpha_c = \sqrt{2\delta}, \tag{8}$$

$$\delta = \frac{N_A\rho_{el}\lambda^2 r_o}{2\pi}, \tag{9}$$

N_A is Avogadro's number, ρ_{el} is the molar electron density (moles of electron per cm^3), and r_0 is the classical electron radius (2.82×10^{-13} cm) (note: there is a misplaced parenthesis in the expression corresponding to Eq. (6) in the following discussion in Ref. [9], and the expressions corresponding to Eqs. (6) and (7) in Ref. [19] have typographical errors). At most of the angles used in our measurements ($\alpha \geq 1°$), τ as determined by Eq. (4) is unreasonably large ($(\alpha^2 - \alpha_c^2) \gg \beta$), and hence only Eq. (2) was used.

The data presented here shows variation in structure as a function of the irradiated depth (τ). Whereas τ-profiles can be measured by varying the incident beam angle α, the true depth profile, the z-profiles, are not so easily measured. What is desirable, for example, is the structure at the interface between two polymer layers. GID can be used to derive the structure at a given z value by suitably subtracting the contribution of all the layers above and below the interface. Such analyses, which are not discussed here, can be carried out by using Laplace transformations [7].

3. Results and discussion

In the various diffraction scans presented here, the scattered intensities are plotted as a function of the scattering angle 2θ at several angles of incidence (α). In scans at low values of α, because of the shallow angle of incidence, the incident beam will be absorbed at the surface layers and hence the contribution to the scattered intensities for the polymer far below the surface or skin will be minimized, thus enhancing the contribution from the surface layers. The contribution from the layers below the surface increases with increase in α, i.e. with increase in the depth of penetration τ, as given in Eq. (2). The thickness of the skin sampled at low α depends on the elemental composition of the surface layer, and is typically on the order of microns for materials with light elements.

3.1. Nylon 6 film (20 μm)

The data were obtained from both sides (the surface in contact with the casting-roll and the surface exposed to air) of a biaxially oriented film. The film is about 45%

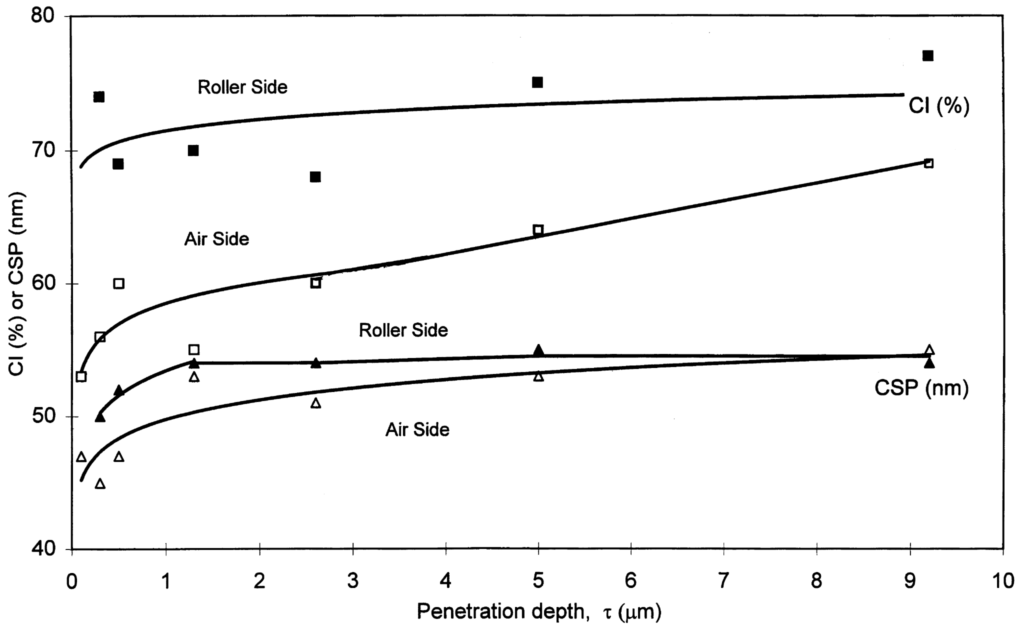

Fig. 3. Variation in the crystalline index (CI) and the crystallite size and perfection (CSP) with the depth of penetration in cast nylon 6 film. The full lines are trend lines obtained by least-squares fit.

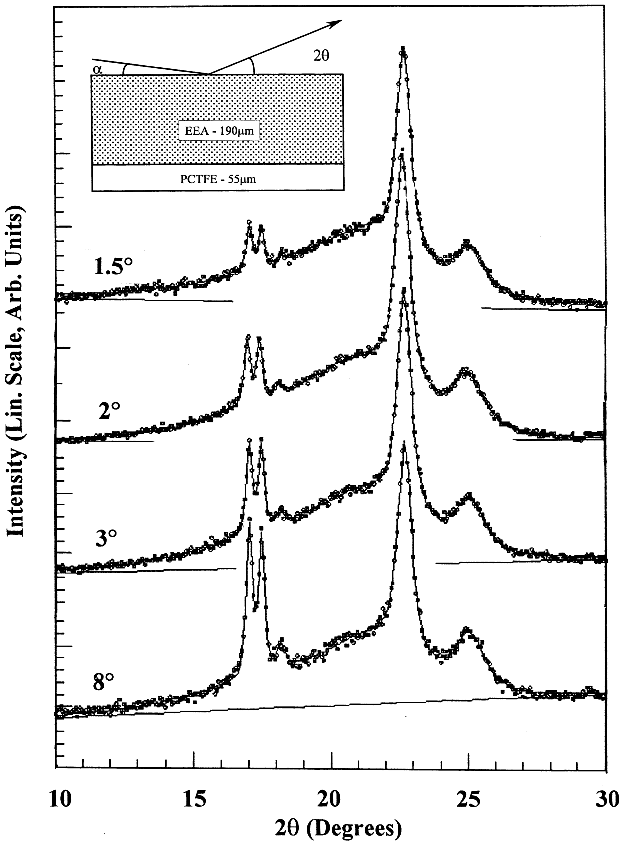

Fig. 4. Examples of the 2θ scans from a EEA/PCTFE laminate at four incident (α) angles. The penetration depths corresponding to these α values are, respectively: 61, 80,114 and 231 μm in PE and 12, 16, 22 and 37 μm in PCTFE.

crystalline and the crystalline fraction is in the α form. The bi-directional orientation of the film aligns the crystallites so that the hydrogen-bonded sheets within the crystal, the (200) planes, are oriented parallel to the surface of the film, but are randomly pointed within this surface. Although N6 has two intense equatorial reflections (the (200) at $2\theta \sim 21°$ and the (002) + (202) and $2\theta \sim 25°$), because of the planar orientation and the reflection geometry used in these measurements, only the (200) reflection is observed. The analysis of the data is illustrated in Fig. 2(a). The results of these analyses are plotted in Fig. 3 showing the variation in crystalline index (CI) and crystallite size and perfection (CSP) as a function of penetration depth τ.

As the crystalline domains are much more highly oriented than the amorphous domains [20], the CI in these analysis is considerably higher than the true CI (~45%). However, the variation in true CI does follow the apparent CI shown in Fig. 3. The plot shows that CI and the CSP on the air-side is lower than on the casting-roll surface. This difference is at first puzzling because the film surface is expected to be quenched to a lower crystalline state at the casting roll (which is cooled with water at a preset temperature of ~10°C) than the surface exposed to air (which is cooled more slowly to the ambient temperature of ~22°C). It could be that the roll-surface could indeed be less ordered than the air-surface immediately after casting. However, subsequent drawing occurs after plasticization with water and at a high temperature of ~100°C. Thus, the initial lower crystalline order at the roll-surface might favor a higher degree of plasticization and development of higher crystallinity than the air-surface in the final drawn film.

The CI at the casting surface is almost constant, suggesting that within the sensitivity of our measurement,

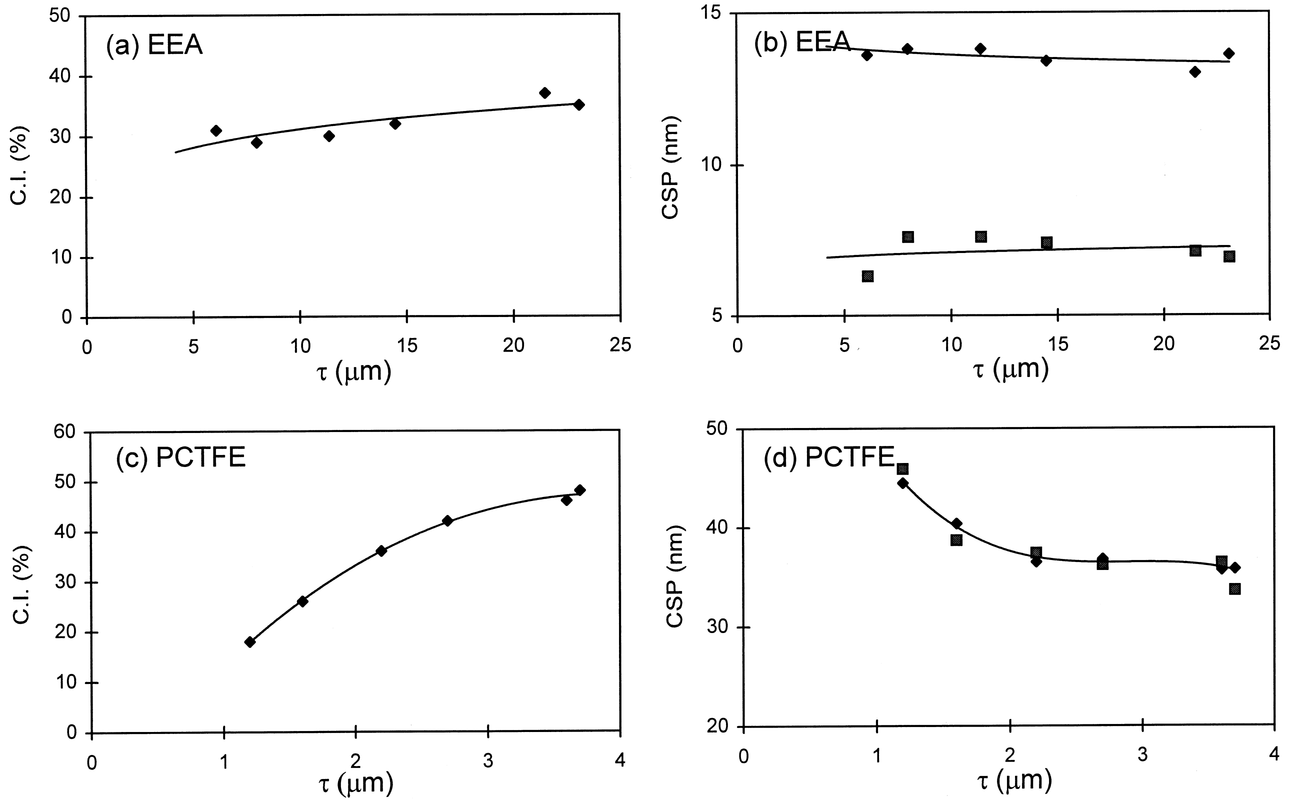

Fig. 5. Variation in the CI and CSP of EEA (a and b) and PCTFE (c and d) layers with depth of penetration. The full lines are trend lines obtained by least-squares fit.

the crystallinity at the casting surface is about the same as that of the core. In contrast, the air-side CI increases dramatically with depth at <1 μm from the surface, at a slower rate at depths >2 μm, and eventually (at ~10 μm) reaches the value at the roll-surface with increased contribution from the core of the film. Similar behavior is observed in the variation in CSP with depth thus confirming that the skin on the air-side is more disordered than that on the side adjacent to the casting roll. Note that the range of CSP values is much smaller than that of CI, and this is perhaps because the largest crystallite size in nylon is typically about 70 Å.

During this study, we wanted to see if there is any morphological basis for the known increase in the surface energy of N6 upon corona treatment (from 54 to 62 dynes/cm). The resulting improvement in the adhesion of ink to the substrate is usually attributed to changes in surface chemistry. Our data showed no significant changes in either the CI or the CSP between the untreated and the corona treated (casting roll side on a commercial line) films. Nevertheless, the data demonstrate that GID can be used to monitor the changes in the surface structure as a result of the variations in the temperatures on either side of the film during casting.

3.2. EEA/PCTFE laminates (190/55 μm)

Fig. 4 shows a series of XRD scans obtained at various α. The data were analyzed as shown in Fig. 2(b), and the results are plotted in Fig. 5 as a function of depth of penetration. The crystalline peaks at 2θ between 15 and 20°, and the underlying amorphous scattering, is primarily due to PCTFE, and that between 20 and 30° to EEA. The diffraction pattern of EEA in this angular range is similar to that of polyethylene. In a conventional parafocus scan, both the EEA and PCTFE peaks are seen from the EEA side and only PCTFE peaks are seen from the PCTFE side. The PCTFE peaks are attenuated in GID scans when samples are mounted so as to expose the EEA side to the beam. The intensity of the PCTFE peaks increases with increasing α: from 1% at 1° ($\tau < 10$ μm; too noisy and hence not shown) to 23% at 8° ($\tau \sim 40$ μm). The results also show that the crystallinity of PCTFE increases from the skin at the interface to the core, but the crystallite size decreases (Fig. 5). The CSP of EEA from the (110) reflection is higher than that of from the (200) reflection, but both show very little change with depth. The CSP from the two intense peaks of PCTFE, (102) and (103), are plotted in the figure, and the two values overlap each other.

The crystallinity and the crystallite sizes of EEA remain essentially constant from skin to core. The EEA data clearly show that the increase in the crystallite size with depth observed for PCTFE is not due to instrumental artifacts such as broadening of the foot-print of the beam at lower α. While the crystallinity of PCTFE increases with depth as

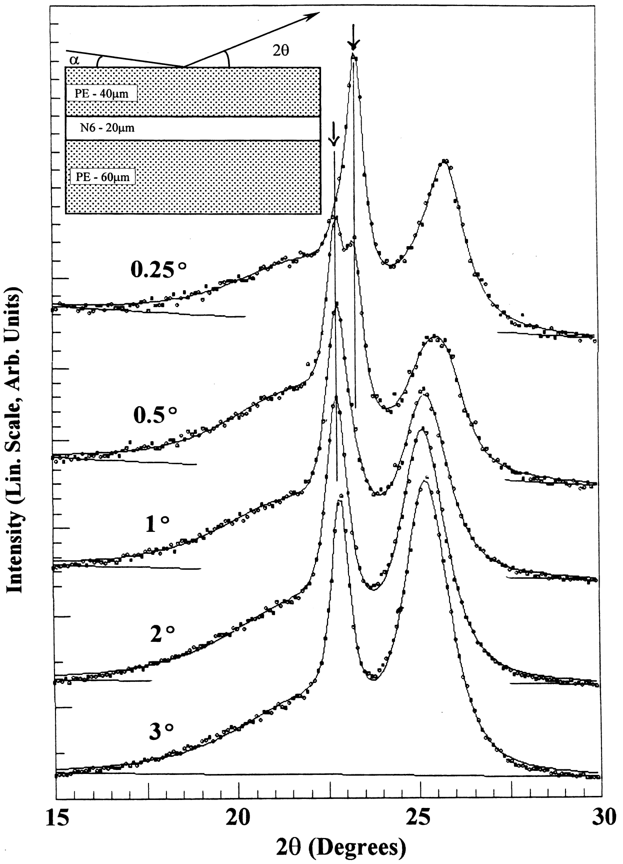

Fig. 6. Examples of the 2θ scans from PE/N6/PE laminate at five incident angles (α). The depths of penetration at these angles are, respectively: 11, 21, 42, 80 and 114 μm in PE and 7, 13,26,50 and 72 μm in N6.

in the case of N6 discussed earlier, the decrease in CSP on PCTFE with increase in depth is opposite to that observed with N6. The higher crystallinity at the core, as in the case of N6, is due to the slow cooling of the interior. But, the higher CSP at the surface could be due to the secondary crystallization resulting from annealing limited to the surface layer during the lamination process.

3.3. PE/N6/PE films (40/20/60 μm)

The inset in Fig. 6 shows the sandwich construction of this laminate and the data from the laminate are shown in the main figure. An example of the analysis of the data is shown in Fig. 2(c). The peak at ~23° is the (110) reflection of PE, and that at $2\theta \sim 25^\circ$ is a combination of the (200) reflection of PE and the (200) + (202) reflection of N6. The N6 is biaxially oriented and hence, as in the first example discussed earlier, only the (002) + (202) reflection at 25.4° (not the (200) reflection at 20°) is seen in these scans. Ideally, two amorphous halos, one for PE at $2\theta \sim 20^\circ$ and the other for N6 at ~21.5°, are required in profile fitting the data of the type shown in Fig. 2(c). But in practice, it is difficult to distinguish between these two broad peaks (full-width at half-maximum = 4–6°) of PE and N6. Therefore, only one amorphous halo is used to account for the scattering from the amorphous segments of N6 and PE. Despite this approximation, the results presented here can still be meaningful with the caveat that the CIs are only relative values. The total crystallinity at all α remains about the same at ~50%.

The crystalline peaks at $2\theta \sim 23^\circ$ and 25° in the scan at $\alpha = 0.25^\circ$ are from the upper PE layer, with a small contribution from N6 to the 25° peak. The intensity of the peak from the N6 layer increases with increasing penetration depth. The scan at $\alpha = 0.5^\circ$ has two PE peaks: the (110) PE reflection at 23.4° from the surface exposed to air, and that at 22.8° from the PE surface adjacent to N6. At higher angles of incidence, the PE peak at $2\theta = 23.4^\circ$ is replaced by the one at $2\theta = 23.4^\circ$. Presence of two (110) peaks at $\alpha = 0.5^\circ$ is accompanied by broadening of the (200) reflection at ~25°. At $\alpha > 1^\circ$, the contribution to the 25° peak is primarily for the N6 layer. Two sets of (110) and (200) PE peaks indicate that there are two different PE unit cells. The two cell dimensions are not from the two PE layers on either side of N6 because: (1) the 25° peak at 0.25° α is weak indicating that the primary contribution to this scan is from the PE layer on the side exposed to the X-ray beam with only a small contribution from the N6 layer and (2) PE scans obtained from both sides of the layer at $\alpha = 0.3^\circ$ (not shown here) were similar. Thus, the PE unit cell is smaller at the air–PE interface than in the bulk or the PE–N6 interface. This difference in the unit cell dimension can be attributed to the differences in the thermal histories of the two surfaces of the PE layer. The implications of this gradient in the crystalline structure on the performance of the film are yet to be determined. Nevertheless, the data demonstrate the utility of the GID technique in detecting the changes in the structure at the interfaces.

3.4. N6/Al/N6/EEA laminates (20/65/20/60 μm)

The XRD scans are shown in Fig. 7, and the data were analyzed as shown in Fig. 2(d). The scans obtained with the N6 side exposed to X-ray beam show the 25° reflection from biaxially oriented N6. A reflection due to a surface coating is seen in scans at small α, suggesting that the additive is entirely on the surface, and this peak is almost absent in the 7° scan. A comparison of the scan obtained at low incidence angles with that obtained in a conventional parafocus scans (which are similar to that obtained at $\alpha = 7^\circ$) best illustrates the usefulness of GID in industrial applications in the identification of thin surface coatings. Comparison of the scans in Fig. 7(b) at $\alpha = 0.3^\circ$ and 7° show that it is possible to analyze the crystallinity, crystal size and other parameters of the PE layer with little interference from the underlying N6 layer.

The scans obtained with X-rays incident on the EEA side also shows a surface coating on the surface of the film at very small incidence angles. The N6 signal is essentially blocked out by the EEA layer at $\alpha = 0.3^\circ$. At higher angles

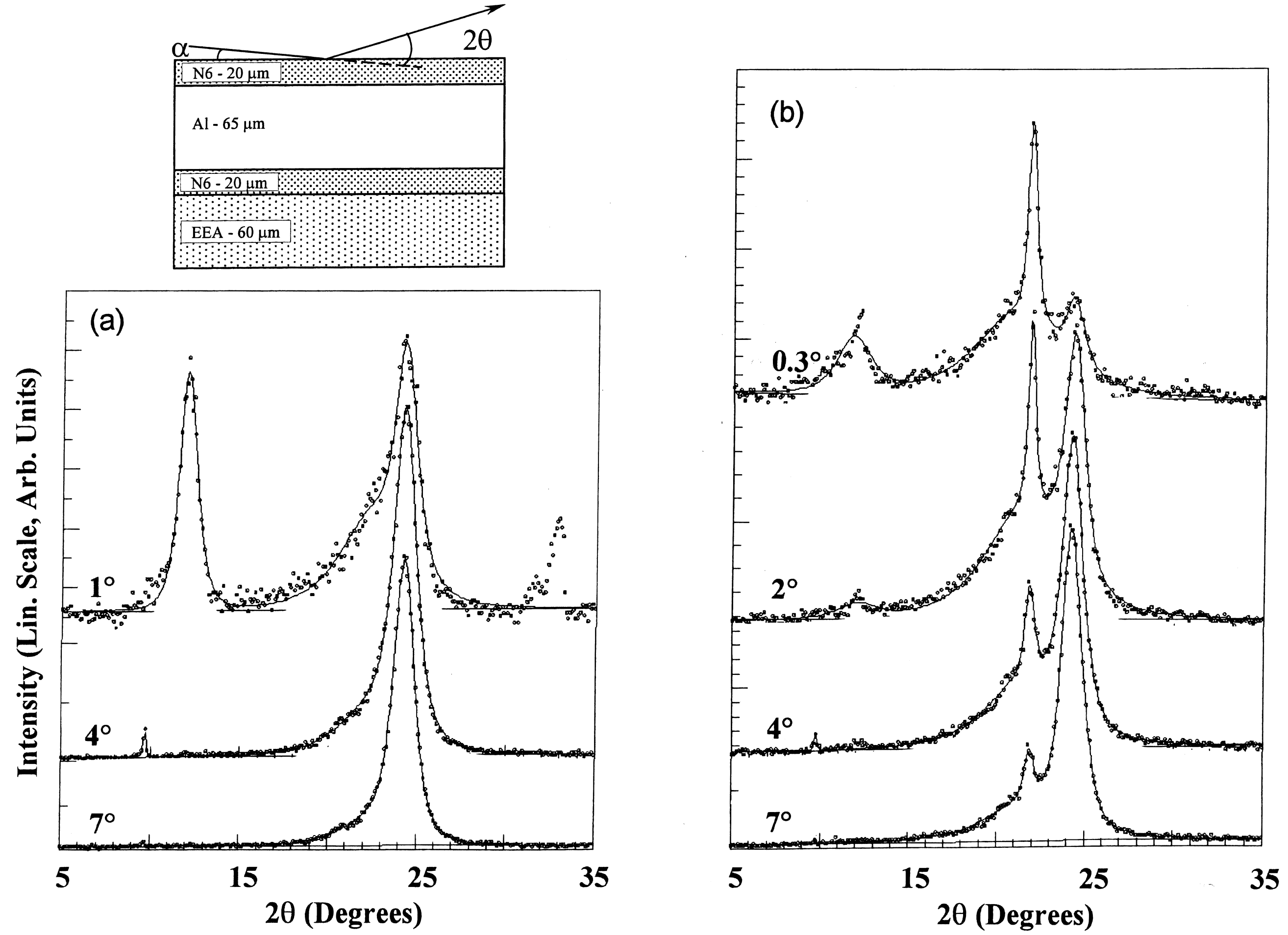

Fig. 7. Examples of the 2θ scan at various incident angles (α) from a N6/Al/N6/EEA laminate. The penetration depth at these α values can be estimated from the previous figures for PE and N6, and are given in Fig. 8 for Al.

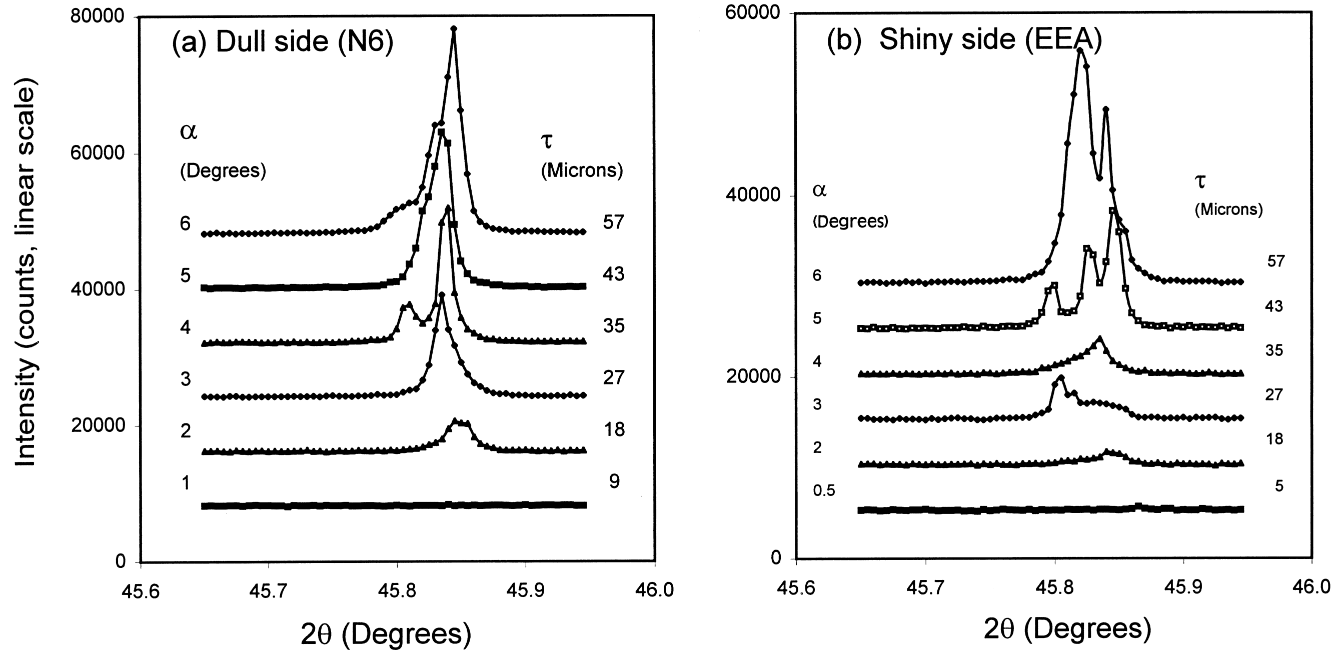

Fig. 8. Variation in the profile of the aluminum peak with depth in the N6/Al/N6/EEA laminate. (a) From the N6 (dull) side. (b) From EEA (shiny) side.

of incidence, the scans show the peaks from EEA and biaxially oriented N6. There is no shift in the EEA peak as was seen in the PE/N6/PE laminates. The 25° peak is due to EEA at $\alpha \leq 1°$, and to N6 at $\alpha > 1°$. The intensity of the N6 peak increases relative to that of EEA at high α.

The XRD scans at higher scattering angles (Fig. 8) show the aluminum signal at 45.8° 2θ is not present at $\alpha \leq 1.0°$ on both the EEA and N6 side of the film. Even a 20 μm layer is sufficient to block out the scattering from aluminum at these low α. On the N6 side, the aluminum peak increases from 25 000 counts at $\alpha = 2°$ to 120 000 at $\alpha = 5$–6°. On the EEA side, the intensity of the aluminum peak increases from 1000 counts at $\alpha = 1°$ to 10 000 at $\alpha = 7°$. The changes in the peak shapes of the aluminum reflections with α show the preferential orientation of aluminum changes with depth.

4. Conclusions

Glancing incidence diffraction (GID) measurements are required for complete structural characterization of films, especially multilayer films. The results are valuable for studying the inhomogeneities in the film induced during processing. Such studies can lead to a better understanding of the failure of laminates, such as by warpage, delamination and dimensional changes.

Acknowledgements

We thank Dr. F. Reidinger for his assistance in obtaining these data, Dr. M. Stamm for his comments, Prof. P. Predicki for numerous helpful suggestions in calculating the depth profiles, and Prof. T.P. Russel for directing us to appropriate references.

References

[1] Parratt LG. Phys Rev 1954;95:359.
[2] Vineyard GH. Phys Rev B 1982;26:4146.
[3] Golovin AL, Imamov RM, Melikyan OG. J Appl Cryst 1989;22:406.
[4] Tidswell IM, Rabedeau TA, Pershan PS, Kosowsky SD, Folkers JP, Whitesides GM. J Chem Phys 1991;95:2854.
[5] van der Sluis P. Mat Sci Forum 1994;166–169:141.
[6] Hauk VM, Oudelhoven RWM, Vaessen GJH. Metall Trans A 1982;13A:1239.
[7] Predicki P. Powder Diffraction 1993;8:122.
[8] Factor BJ, Russel TP, Toney MF. Phys Rev Lett 1991;66:1181.
[9] Factor J, Russel TP, Toney MF. Macromolecules 1993;26:2847.
[10] Foster MD. Crit Rev Anal Chem 1993;24:179.
[11] Russel TP. MRS Bull 1996;21:49.
[12] Saraf RF. Langmuir 1996;12:2802.
[13] Russel TP. Mat Sci Reports 1990;5:171.
[14] Lu JR, Lee EM, Thomas RK. Acta Cryst A 1996;52:11.
[15] Stamm M, Schubert DW. Ann Rev Mater Sci 1995;25:325.
[16] Murthy NS, Minor H. Polymer 1990;31:996.
[17] Howard SA. Adv X-ray Anal 1989;32:523.
[18] Guinier A. X-ray diffraction. San Francisco: Freeman, 1963. p. 124.
[19] Predicki P. A practical guide for the preparation of specimens for X-ray fluorescence and X-ray diffraction analysis. In: Buhrke VH, Jenkins R, Smith DK, editors. New York: Wiley–VCH, 1998. p. 236.
[20] Murthy NS, Minor H, Bednarczyk C, Krimm S. Macromolecules 1993;26:1712.